USCAP

ARTICLE

The Notch signalling pathway and miRNA regulation play important roles in the differentiation of Schwann cells from adipose-derived stem cells

Liang Yang[1], Xiang-Min Shen[2], Zhi-Fei Wang[1], Ke Li[2] and Wei Wang[2]✉

An exploration of the underlying mechanisms is necessary to improve nerve myelin-forming cell Schwann cell (SC) differentiation from adipose-derived stem cells (ADSCs). Primary rat ADSCs were isolated and characterised for cell surface markers using flow cytometry analysis. After treatment with a mixture of glial growth factors, ADSCs were induced to differentiate and subsequently identified by immunofluorescence staining and western blotting. A miRNA microarray analysis was performed to explore the genes and signalling pathways regulating ADSC differentiation into SCs. ELISAs were conducted to measure the expression of neurotrophic factors and changes in the level of nerve cell adhesion factor. Dual luciferase reporter assays and RIP assays were performed to explore the potential mechanism of miR-21-5p in ADSC differentiation. The isolated ADSCs were positive for CD29 and CD44 but negative for CD49. After induction with specific cytokines, the differentiated ADSCs presented a spindle-like morphology similar to SCs and expressed S100. RNA-sequencing analyses revealed that 9821 mRNAs of protein-coding genes and 175 miRNAs were differentially expressed in differentiated SC-like cells compared to primary cultures of ADSCs. KEGG and Gene Ontology analyses revealed that the involvement of the Notch signalling pathway and miRNA negative regulation may be associated with the differentiation of ADSCs into SCs. Treatment with a Notch inhibitor promoted the differentiation of ADSCs. Furthermore, mechanistic studies showed that Jag1 bound to miR-21-5p and upregulated its target gene Jag1, thus affecting ADSC differentiation. These results revealed the mechanism underlying the important roles of miRNAs and the Notch signalling pathway in the differentiation of SCs from ADSCs, enabling potential therapeutic applications of ADSCs in peripheral nerve regeneration in the future.

Laboratory Investigation (2022) 102:320–328; https://doi.org/10.1038/s41374-021-00687-2

INTRODUCTION

Schwann cells (SCs), which are recognised as the best seed cells for peripheral nerve tissue engineering, play a crucial role in peripheral nerve regeneration and repair of axonal damage[1,2]. With the development of tissue engineering technology, SCs have also been proposed to repair damage to the central nervous system. However, due to the limited sources and proliferation ability, as well as the difficulty of cell culture in vitro[3,4], the rapid generation of a sufficient number of SCs that fully meet the requirements and characteristics of seed cells for clinical application is difficult.

Adipose-derived stem cells (ADSCs), on the other hand, have the advantages of being easily obtained from extensive sources, easy cultivation and causing little injury to the donor[5,6]. Under certain conditions, ADSCs differentiate into various tissues, such as osseous tissue[7], cartilaginous tissue[8], adipose tissue[9], myeloid tissue[10] and nervous tissue[11], indicating that they are ideal seed cells for tissue engineering. The phenotypic and gene expression profiles of ADSCs are similar to those of bone marrow mesenchymal stem cells (BMSCs)[12–15], which are both derived from the embryonic mesoderm and express similar surface markers. ADSCs are able to differentiate into neural cells under appropriate induction conditions[16]. According to previous studies, ADSCs are induced and differentiated into SC-like cells, which are identical to true SCs in terms of morphology, surface markers and functions of promoting myelin growth[17–22]. ADSCs may become a reliable and abundant source of differentiated SCs and play an important role in nervous system regeneration and axonal injury repair.

In the present study, we successfully isolated ADSCs from adipose tissue and induced their differentiation into SC-like cells. We subsequently performed RNA sequencing on differentiated and primary cultured ADSCs. Based on a statistical analysis of differentially expressed genes and signalling pathways, we discovered that the Notch signalling pathway inhibited the differentiation of ADSCs into SCs. Finally, we proposed a molecular mechanism by which miR-21-5p might regulate the differentiation of ADSCs into SCs.

MATERIALS AND METHODS

Animals

Adult male Sprague–Dawley rats weighing approximately 250 g were purchased from SJA Laboratory Animal Co., Ltd. (Hunan, China). All animals utilised in this study received care according to the policies and principles

[1]Department of Neurosurgery, The Third Xiangya Hospital of Central South University, Changsha 410078, P.R. China. [2]Department of Neurology, The Second Xiangya Hospital of Central South University, Changsha 410011, P.R. China. ✉email: 505034@csu.edu.cn

Received: 16 December 2020 Revised: 14 October 2021 Accepted: 15 October 2021
Published online: 18 November 2021

established by the Animal Welfare Act and the NIH Guide for the Care and Use of Laboratory Animals.

Isolation and culture of ADSCs

Rats were euthanized by an intraperitoneal injection of 10% chloral hydrate anaesthesia (0.5 ml/100 g). After immersion sterilisation in 75% alcohol, bilateral inguinal fat pads were carefully dissected and minced after washes with phosphate-buffered saline (PBS) and digested three times with 5 ml of trypsin at 37 °C for 10 min. The digestion solution was passed through a 200-mesh filter to remove undissociated tissue, neutralised with low-glucose Dulbecco's modified Eagle's medium (DMEM) o containing 20% (v/v) foetal bovine serum (FBS) (Gibco, USA) and then centrifuged at 1000 r/min for 5 min. The supernatant was removed, and the stromal cell pellet was resuspended in low-glucose DMEM containing 20% (v/v) FBS and a 1% (v/v) penicillin/streptomycin solution, followed by inoculation in a T25 flask at a density of 4×10^5 cells/ml and an incubation at 37 °C with 5% CO_2. The medium was renewed after 48 h, and the nonadherent cells were removed to obtain F0 generation cells. After passage and expansion culture, third- to fifth-generation ADSCs were induced to differentiate. Frozen stock solutions of 80% DMEM/F12 containing 10% FBS and 10% DMSO were used to preserve the ADSCs.

Characterisation of ADSC surface markers using flow cytometry

Rat ADSCs within three to five passages were harvested by trypsinization and subsequently fixed with neutralised 4% paraformaldehyde for 30 min. The fixed cells were washed twice with PBS and then incubated with the following antibodies at 4 °C for 30 min: hamster fluorescein isothiocyanate (FITC)-conjugated CD29, mouse PE-conjugated CD44 and mouse allophycocyanin-conjugated CD49 from eBioscience, Inc. (San Diego, CA, USA). Flow cytometry was performed with a FACScan flow cytometer (Becton Dickinson, San Jose, CA).

Induction of ADSC differentiation into SC-like cells

Growth medium was removed from subconfluent ADSC cultures at the fourth passage and replaced with preinduction solution (DMEM/F12 containing 20 ng/ml EGF, 20 ng/ml basic fibroblast growth factor (bFGF) and 2% B27). Cells were cultured in a 37 °C incubator with 5% CO_2 for 7 days with fresh medium changes every 2–3 days. The blank control solution was DMEM/F12 containing 10% FBS. After 7 days of preinduction, cells were seeded into a 6-well plate precoated with laminin. Subsequently, the preinduction solution was removed and replaced with SC-conditioned differentiation medium (DMEM/F12 containing 10% FBS, 14 μM forskolin (Alexis Biochemichals, San Diego, CA, USA), 5 ng/ml platelet-derived growth factor-AA (PeproTech, Rocky Hill, NJ, USA), 10 ng/ml bFGF (PeproTech) and 200 ng/ml recombinant human heregulin-β1 (PeproTech)). Cells were cultured in a 37 °C incubator with 5% CO_2 for 9 days with fresh medium added every 2–3 days. The blank control was DMEM/F12 containing 10% FBS.

As a method to determine the role of Notch signalling in cell differentiation, ADSCs were treated with the Notch1 inhibitor tangeretin (Sigma) at 25 mM to inhibit cleavage of the Notch intracellular domain, thus inhibiting the Notch signalling cascade.

Identification of Schwann-like cells

For the immunocytochemical assessment of the expression of markers of differentiated ADSCs, the ADSCs were cultured in SC-conditioned medium for 12–14 days and then fixed with 4% (W/V) paraformaldehyde for 30 min. The fixed cells were blocked with goat serum for 1 h at room temperature. The rabbit polyclonal primary antibodies against GFAP (1:200; ab4648), S100 (1:200; ab52642), SOX2 (1:200; ab92689), c-Myc (1:200; ab32072), OCT4 (1:200; ab181557) and KLF4 (1:200; ab214666) from Abcam (Cambridge, MA, USA) were added and incubated at 4 °C overnight. Following the incubation, Cy3- (1:100; SA00003-2) or FITC-conjugated (1:100; SA00009-2) goat anti-rabbit secondary antibodies (Proteintech Group, Inc., Chicago, IL, US) were added and incubated at 37 °C for 1 h. The cell nuclei were labelled with DAPI (Sigma). PBS was substituted for primary antibodies as a control. The cells were visualised and recorded using a fluorescence microscope (Nikon Eclipse 80i).

For western blot analyses, fourth passage rat ADSCs were harvested by trypsinization, and 1×10^6 cells/ml were mixed with 100 μl of protein isolation buffer, followed by centrifugation at 12,000 g for 30 min at 4 °C. Lysed cells were incubated for 15 min on ice and then subjected to two freeze–thaw cycles prior to the analysis of the protein content using a commercially available protein assay kit (Bio-Rad, UK). Thirty micrograms of protein was prepared from each sample, combined with Laemmli buffer and denatured at 95 °C for 5 min. The proteins were resolved on 15 or 12% SDS–PAGE gels (Beijing Dingguo Biotech, Co., Ltd.) and transferred onto PVDF membranes. The membranes were blocked for 1 h with 5% bovine serum albumin and then incubated overnight at 4 °C with primary antibodies against S100, GFAP, SOX2, c-Myc, OCT4, KLF4, Jag1 (1:100; ab7771; Abcam) and Hes1 (1:100; ab71559). The membranes were incubated for 1 h at 37 °C with HRP-conjugated secondary antibodies [goat anti-mouse and goat anti-rabbit (1:1000; Cell Signalling Technology, USA)]. Antibodies were stripped from the membranes using 100 mM glycine, pH 2.9, and the blots were reprobed with a β-actin antibody (1:1000; Abcam, UK) as a loading control. The blots were scanned using a ChemiDoc XRS + image analysis system (Bio-Rad Laboratories, Inc., Hercules, CA, USA) and analysed using ImageJ software (National Institutes of Health, Bethesda, MD, USA).

Cell transfection

Genema (Shanghai, China) synthesised miR-21-5p and miR-NC. The vector containing the Rbpj 3′-untranslated region (UTR) fragment containing putative binding sites for miR-21-5p was synthesised by GeneChem (Shanghai, China). Cells (5×10^5) were plated in 6-well plates 24 h prior to transfection with the Rbpj 3′UTR-WT/Mut overexpression plasmid, miR-21-5p and miR-NC at 60–70% confluence and then transfected using Lipofectamine 2000 (Invitrogen, Carlsbad, CA, USA). Forty-eight hours after the transient transfection of plasmids, cells were harvested for further experiments.

mRNA extraction and RT-qPCR analysis

Total RNA was isolated from control ADSC cultures and ADSCs in the fourth passage using RNA Isolator Total RNA Extraction reagent (Vazyme, Piscataway, NJ, USA). The expression of mRNAs was detected using an Ace-Hi^{TM} One Step Quantitative Real-Time PCR SYBR Green kit (cat. no. Q221-01; Vazyme), and qRT-PCR was performed using an LCS 480 real-time PCR system, according to the manufacturers' protocols. The primers sequences are shown in Table 1. The reaction conditions were set as denaturation for 1 min at 94 °C, primer annealing for 1 min at 60 °C and chain elongation for 1.45 min at 72 °C on a DNA thermocycler (MJ Mini personal thermocycler, Bio-Rad). The relative expression of each mRNA was calculated using the $2^{-\Delta\Delta Cq}$ method and normalised to that of the GAPDH mRNA for each data point.

RNA sequencing and analysis[23]

The integrity of total RNA was assessed using Bio-Rad Experion. Sequencing libraries were prepared with the TruSeq Stranded mRNA Kit (Illumina). On-board cluster generation using the TruSeq Rapid SR Cluster Kit-HS (Illumina) and single-read 50 nt sequencing were performed with a HiSeq Rapid SR Flow Cell (Illumina) using the Illumina 1500 platform.

Illumina output bcl files were converted and demultiplexed using the Illumina bcl2fastq script, version 1.8.3. Sequenced reads were aligned to the *Mus musculus* Ensembl reference genome (release 74, GRCm38) using STAR[24].

Gene read counts were established as read counts within merged exons of protein-coding transcripts (for genes with annotated protein gene products) or within merged exons of all transcripts (for noncoding genes). Fragments per kilobase per million (FPKM) were based on the total raw read count per gene and length of merged exons. Differential expression was assessed for genes with a minimum FPKM value of 0.3 in 1 sample using DEseq2[25]. Thus, derived p values were subjected to Benjamini–Hochberg adjustment to correct for multiple hypothesis testing. We considered genes as differentially expressed if a fold change of 2 or 1.5 was observed (indicated in the text) with an adjusted p value of 0.05 to also include smaller differences in expression between conditions.

RNAseq data have been deposited in the EBI ArrayExpress archive (http://www.ebi.ac.uk/arrayexpress/) and are accessible via the accession number E-MTAB-5600.

ELISA

Cell lysate samples were prepared, and 100 μl of samples in coating buffer was added to the wells of a microtiter plate. After an overnight incubation at 4 °C, the samples were removed and washed with PBST buffer three times. The coated wells were then blocked with 100 μl of 3% skim milk in

Table 1. Paired primer seqTences Tsed in qRT-PCR.

Genes	Paired primers	SeqTences (5′-3′)
SOX2	Sense	CATGAAGGAGCACCCGGATT
	Antisense	CATCATGCTGTAGCTGCCGT
C-myc	Sense	TCCTGTACCTCGTCCGATTC
	Antisense	GGTTGCCTCTTTTCCACAGA
Oct4	Sense	AGGTGGAACCTAGTCCCGA
	Antisense	GGTTGTCTGGCTGAACACCTT
KLF4	Sense	AGTTTACCTCCGACCCCATT
	Antisense	AAGGCTTTTCTCCTGGCTTC
Jag1	Sense	GGCTACTCAGGACCGAACTG
	Antisense	CTTGGCCTCGCACTCATTTG
Hes1	Sense	GAAAGATAGCTCCCGGCATT
	Antisense	GTCACCTCGTTCATGCACTC
GFAP	Sense	GCTCCAAGATGAAACCAACC
	Antisense	CCAGCGACTCAACCTTCCT
S100	Sense	CTTGATTTGCTTCAGGGATGA
	Antisense	CCCACAGAGTGTTGATTTCG
GAPDH	Sense	GCAAGTTCAACGGCACAG
	Antisense	GCCAGTAGACTCCACGACAT
let-7-5p	RT	GTCGTATCCAGTGCAGGGTCCGAGGTATTCGCACTGGATACGACAACTAT
	Sense	TGAGGTAGTAGGTTGTATGGTT
miR-30-5p	RT	GTCGTATCCAGTGCAGGGTCCGAGGTATTCGCACTGGATACGACCTTCCA
	Sense	GGCGTGTAAACATCCTCGAC
miR-34-5p	RT	GTCGTATCCAGTGCAGGGTCCGAGGTATTCGCACTGGATACGACACAACC
	Sense	GCCTGGCAGTGTCTTAGCT
miR-127-3p	RT	GTCGTATCCAGTGCAGGGTCCGAGGTATTCGCACTGGATACGACAGCCAA
	Sense	GCTCGGATCCGTCTGAGC
miR-21-5p	RT	GTCGTATCCAGTGCAGGGTCCGAGGTATTCGCACTGGATACGACTCAACA
	Sense	CGCGCTAGCTTATCAGACTGA
miRNA	Antisense	GTGCAGGGTCCGAGGT
U6	Sense	CTCGCTTCGGCAGCACA
	Antisense	AACGCTTCACGAATTTGCGT

PBS at RT for 1 h. After three washes with PBST buffer, 100 µl of NGF, BDNF, IL-6 and NCAM antibody solutions were added and incubated at RT for 1 h with gentle shaking. All wells were then washed with PBST buffer three times, and then the corresponding secondary antibody was added followed by another 1 h incubation at RT. Finally, the substrate solution was added, the signal was measured and the expression level was calculated.

Signalling pathway analysis

The NCBI FLink site was used to perform the pathway analysis. NCBI gene IDs for either upregulated or downregulated genes were input into the gene database and then linked to the gene biosystem database. The resulting list was downloaded into Excel and filtered for KEGG pathways with at least 15 genes from our list of significant genes and comprised more than 10% of the number of genes in the KEGG database. Then, a hypergeometric test was applied with $p \geq 0.05$ as a cutoff score. The list of significant genes in the significant pathways was downloaded from the FLink page.

Dual luciferase reporter assay

The putative binding sites between miR-21-5p and the Jag1 3′-UTR were predicted by TargetScan. Serial constructs were then generated using the pGL3 luciferase promoter plasmid (Promega Corporation, Madison, WI, USA). Point mutations of the miR-21-5p-targeting sites in the Jag1 3′-UTR were directly synthesised using the QuickChange Multiple Site-directed Mutagenesis Kit (Stratagene, La Jolla, CA, USA). Each plasmid construct was subsequently cotransfected with miR-21-5p mimics, miR-21-5p inhibitors and a corresponding negative control into H9C2 and H293 cells seeded in 12-well plates using Lipofectamine 2000 (Invitrogen, Carlsbad, CA, USA). Forty-eight hours after transfection, cells were harvested, and luciferase activities were detected using the Dual Luciferase Reporter Assay Kit (Promega). The ratio of firefly to Renilla luciferase activity was subsequently determined.

Statistical analysis

Experimental data are presented as the means ± standard deviations of at least three independent replicates after an analysis with GraphPad Prism 5 software (GraphPad Software, La Jolla, CA, USA) and an assessment of comparisons between different groups using Student's *t* test. Differences were considered significant at p values < 0.05.

RESULTS

Isolation and identification of ADSCs

Within three to five passages after initial plating of the primary culture, the ADSCs exhibited a uniformly aligned monolayer of fibroblast-like cells with a swirl or parallel growth style (Fig. 1A; left panel). As the cells approached confluence, they assumed a more spindle-shaped, fibroblastic morphology (Fig. 1A; right panel). The expression of cell surface markers of ADSCs was examined using

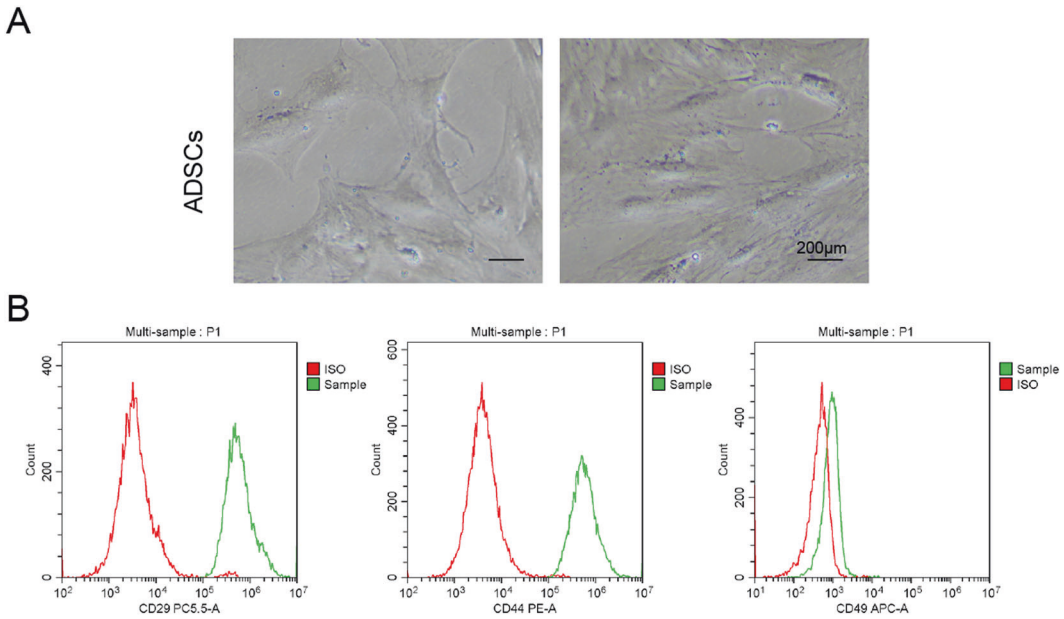

Fig. 1 Characteristics of rat ADSCs. Rat ADSCs were passaged 3–5 times after the initial plating of the primary culture. **A** Under a phase contrast microscope, cultured rat ADSCs were spindle-shaped (scale bar 200 μm). **B** Flow cytometry analysis of rat ADSCs using specific FITC- and PE-conjugated antibodies against the surface markers CD44, CD29 and CD49. An isotype control is included in each test (red lines).

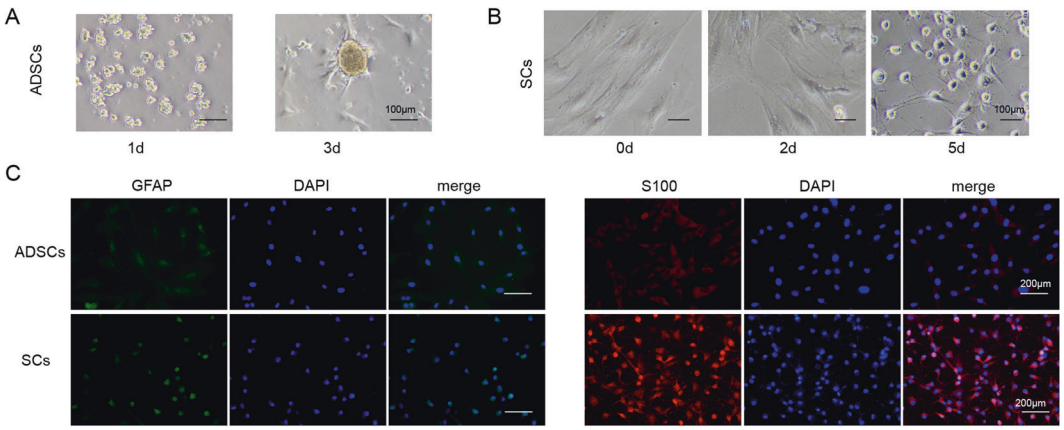

Fig. 2 ADSCs differentiated into SC-like cells. ADSCs were cultured for 9 days on laminin-coated 6-well plates in SC differentiation medium. **A** ADSC sphere formation experiment. **B** Morphology of differentiated ADSCs. **C** Identification of ADSCs before and after induction by immunofluorescence staining for GFAP and S100.

flow cytometry to further characterise these cells. The primary cultured ADSCs expressed CD29 (99.3%) and CD44 (94.3%) but did not express CD49 (1.3%) (Fig. 1B), indicating the successful isolation of primary rat ADSCs.

Induction of ADSC differentiation into SC-like cells

The results of the sphere formation assay revealed an increased proportion of small spheres of floating cells after 1 day. The ADSCs transformed from a monolayer of large cells with a flat morphology to a small number of bipolar or tripolar spindle-like shaped cells (Fig. 2A; upper panel). Three days after differentiation, the size of the cell spheres was markedly increased (Fig. 2A; lower panel), indicating that the experimental conditions and operation methods met the requirements. Differentiated ADSCs exhibited morphological changes similar to those of SCs, including a decrease in cell volume, a monolayer of long, spindle-shaped fibroblasts, greater three-dimensionality and hyalomeres present in the periphery of the cell (Fig. 2B). Immunofluorescence staining showed that less than 5% of differentiated ADSCs were positive for GFAP, while approximately 90% of induced human ADSCs were positive for S100 (Fig. 2C).

Expression of differentiation-associated genes

We further examined the expression of differentiation-associated genes before and after ADSC differentiation induction. The results from IF (Fig. 3A) and western blotting (Fig. 3B) revealed decreased levels of SOX2 and KLF4 and increased levels of C-myc and OCT4 in differentiated ADSCs, suggesting the success of ADSC differentiation into SC-like cells.

RNA sequencing and differential expression analysis

We performed a genome-wide transcriptome analysis of differential gene expression between differentiated and primary cultured ADSCs using RNA-sequencing (RNAseq) technology to explore the genes and signalling pathways that regulate ADSC differentiation into SCs. The volcano plot of differentially expressed genes shows 9821 protein-coding mRNAs that were significantly different, with 4819 upregulated and 5002 downregulated in SCs versus primary

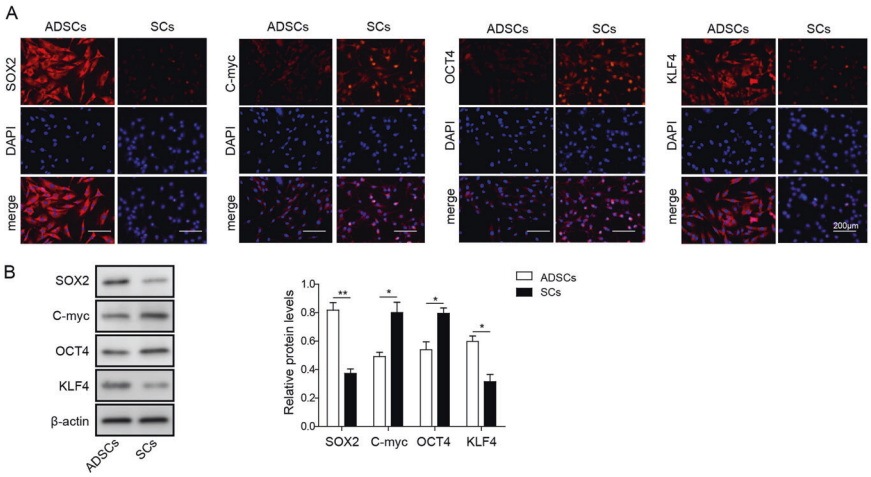

Fig. 3 Expression of differentiation-associated genes before and after induction. A Immunofluorescence staining for SOX2, c-Myc, OCT4 and KLF4. **B** Western blots showing the levels of the SOX2, c-Myc, OCT4 and KLF4 proteins.

cultured ADSCs (Supplementary Fig. S1A). Similarly, the unsupervised two-dimensional hierarchical clustering analysis of differentially expressed genes clearly separated the differentiated and primary cultured ADSCs (Supplementary Fig. S1B). The most significantly upregulated genes Mylk, Ccdc80 and Myh10 and downregulated genes Cd24, Gfpt2 and Mmd may play important roles in the differentiation of ADSCs into SCs (Supplementary Fig. S1C). KEGG pathway analysis revealed the participation of differentially expressed genes in multiple cellular signalling pathways, including the focal adhesion and proteoglycan signalling pathways that are involved in the regulation of cell motility (Supplementary Fig. S2A). Gene Ontology analysis revealed a significant change in the Notch signalling pathway, with functional protein-coding genes, including Jag1 and Hes1, expressed at lower levels in differentiated and primary cultured ADSCs (Supplementary Fig. S2B, C). The small noncoding RNA analysis also identified 175 miRNAs (169 upregulated and 6 downregulated) that were differentially expressed in primary cultured ADSCs compared with SC-like cells differentiated from ADSCs (Supplementary Fig. S3A). Target prediction using TargetScan for these differentially expressed miRNAs indicated that they may be upstream regulatory factors in the Notch pathway (Supplementary Fig. S3B and Supplementary Table S1), further suggesting the importance of this pathway in the process of ADSC differentiation into SCs.

Verification of RNAseq results

We examined the intrinsic mRNA expression of DEGs involved in the Notch signalling pathway using RNAseq to determine the potential importance of the Notch pathway in ADSC differentiation into SCs. Among known negative regulators, we observed the downregulation of Jag1, which encodes a Notch ligand, and Hes1 in rat ADSCs cultured in differentiation medium (Fig. 4A). Consistent with their transcript levels, Jag1 and Hes1 proteins were essentially undetectable in ADSCs after differentiation induction, consistent with the sequencing results (Fig. 4B, C). Following target prediction using TargetScan, the expression of several upregulated miRNAs that may target these Notch signalling molecules (Supplementary Table S1) was also verified to increase significantly after differentiation induction (Fig. 4D), showing an obvious negative correlation with the Notch pathway.

We further investigated the functions of the Notch pathway in ADSC differentiation by inhibiting Notch1 with tangeretin. ADSCs were differentiated in the absence or presence of tangeretin, a Notch inhibitor, for a period of 2 weeks and then assessed using immunocytochemistry and western blot analysis for the expression of glial GFAP and S100 proteins. We observed a more pronounced contraction and more elongated protrusions in induced ADSCs incubated with the Notch1 inhibitor, indicating enhanced differentiation into SCs (Fig. 4E). The addition of tangeretin efficiently promoted the expression of the S100 mRNA in SCs, whereas this treatment did not alter GFAP levels (Figs. 4F and 5), suggesting the negative regulatory effect of the Notch pathway on ADSC differentiation into SCs.

miR-21-5p inhibits the Notch signalling pathway by targeting Jag1 and regulates the differentiation of ADSCs into SCs

The binding sites for miR-21-5p in the 3′-UTR of Jag1 were predicted by TargetScan, as shown in Fig. 6A, and the corresponding plasmids were prepared. We tested the binding of miR-21-5p by performing a dual luciferase reporter assay to validate the prediction. As shown in Fig. 6B, the luciferase signal of the wild-type Jag1 3′-UTR plasmid was significantly reduced by the addition of miR-21-5p, strongly suggesting that miR-21-5p bound to the 3′-UTR of Jag1. Furthermore, the formation of the complex of miR-21-5p and the Jag1 3′-UTR was confirmed by RIP pulldown of Ago2 (Fig. 6C). qRT-PCR and western blotting were applied to measure the levels of miR-21-5p and the Jag1 protein, respectively. As shown in Fig. 6D, miR-21-5p mimics increased the miR-21-5p level by over three-fold, and the miR-21-5p inhibitor reduced its level. Regarding the level of the Jag1 protein, the miR-21-5p mimics, which increased the miR-21-5p level, reduced the Jag1 level, while the miR-21-5p inhibitor increased Jag1 levels, as shown in Fig. 6E, indicating the regulatory effect of miR-21-5p on the Jag1 protein level. All these data revealed that miR-21-5p directly targeted and negatively regulated Jag1 expression.

We further investigated the effect of miR-21-5p on the differentiation of ADSCs into SC-like cells by establishing stable Jag1-transfected ADSC lines and added miR-21-5p mimics during the induction process. Jag1 overexpression increased the expression levels of proteins in the Notch pathway and reversed the inhibitory effect of miR-21-5p on the Notch pathway (Fig. 7A, B). Treatment with miR-21-5p mimics decreased Jag1 protein levels and facilitated the differentiation of ADSCs into SC-like cells. The effect was confirmed by the upregulation of C-myc and OCT4 and the downregulation of SOX2 and KLF4, as measured using western blotting (Fig. 7C, D). The ELISA results showed that overexpression of miR-21-5p inhibited β-NGF, BDNF, IL-6 and NCAM expression, but Jag1 overexpression neutralised this effect, explaining the functions of miR-21-5p and Jag1 in the cell differentiation process (Supplementary Fig. S4). Overall, miR-21-5p was involved in the differentiation of ADSCs into SC-like cells by downregulating Jag1 levels and regulating the downstream Notch pathway.

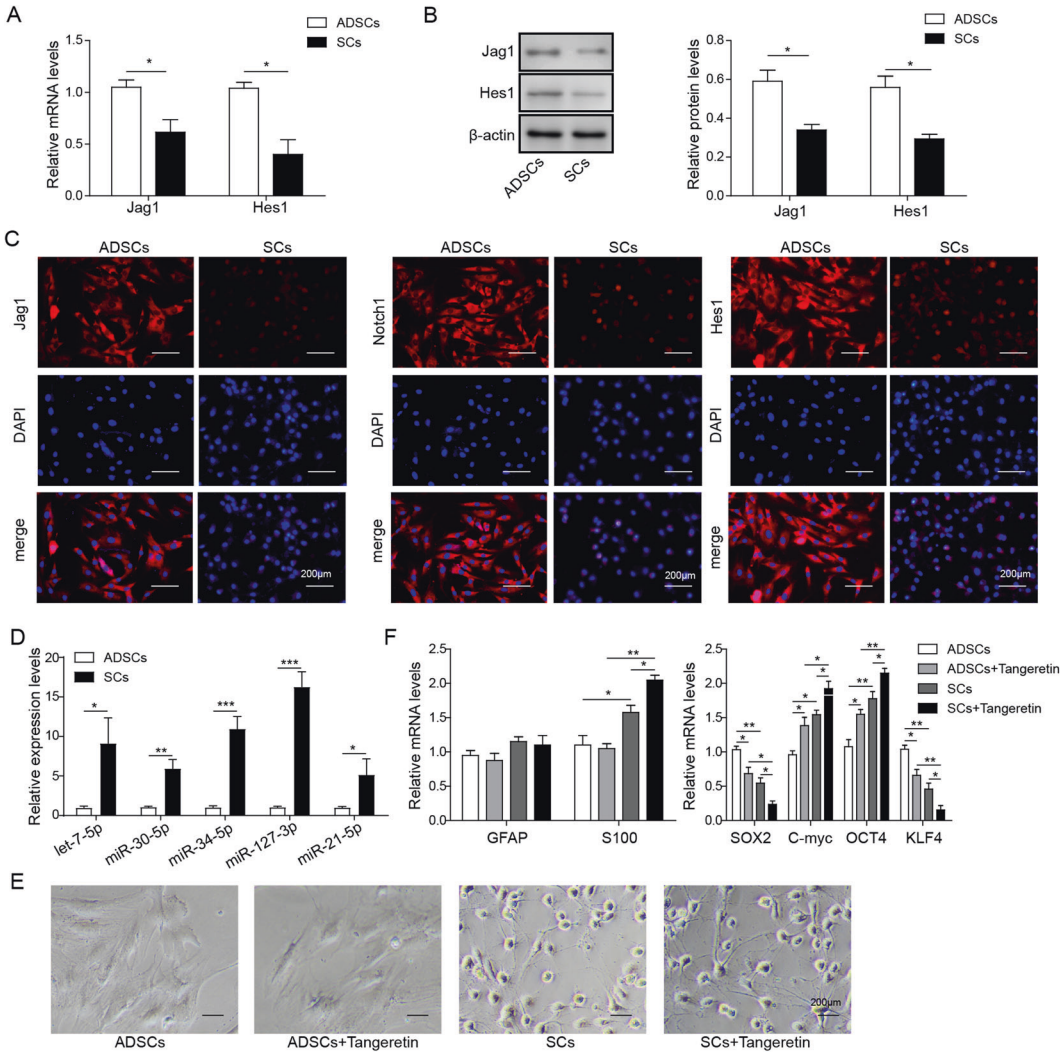

Fig. 4 Verification of RNAseq results. A The mRNA levels of Jag1 and Hes1 in differentiated and primary cultured ADSCs were detected using qRT-PCR. **B** Western blots showing levels of the Jag1 and Hes1 proteins in differentiated and primary cultured ADSCs. **C** Immunofluorescence staining for Jag1, Notch1 and Hes1 in differentiated and primary cultured ADSCs. **D** The expression levels of let-7-5p, miR-30-5p, miR-34-5p and other representative miRNAs in differentiated and primary cultured ADSCs were detected using qRT-PCR. **E** Morphology of differentiated and primary cultured ADSCs treated with or without the Notch1 inhibitor tangeretin. **F** The mRNA levels of GFAP, S100, SOX2, c-Myc, OCT4 and KLF4 in differentiated and primary cultured ADSCs treated with or without the Notch1 inhibitor tangeretin were detected using qRT-PCR.

DISCUSSION

ADSCs are increasingly used in tissue engineering strategies aimed at developing peripheral nerves for reconstructive and regenerative therapies. Despite the remarkable potential harboured within ADSCs, signalling mechanisms controlling ADSCs are poorly understood. In the present study, we successfully induced ADSCs to differentiate into SC-like cells. Furthermore, we elucidated the molecular mechanism by which the Notch signalling pathway mediates this differentiation process using RNAseq for the first time.

ADSCs are multipotent stem cells derived from adipose tissue that exhibit a morphology and multilineage differentiation potential similar to BMSCs[26,27]. On the other hand, ADSCs have many advantages over BMSCs in the study of tissue engineering, including extensive sources, greater accessibility, easier culture and expansion and stronger multilineage differentiation potential[28]. Previous studies have shown that ADSCs differentiate into SC-like cells under appropriate induction conditions[17–22]. For ADSCs to become ideal cells for tissue engineering, they must generate a sufficient number of functional and high-quality neural cells. Therefore, we induced and differentiated ADSCs into SC-like cells using solutions that contained small molecules, growth factors and cytokines. This approach represents an improvement over some of the existing methods in which a single inducer was applied several times[22]. The four transcription factors SOX2, OCT4, C-myc and KLF4 that are required to induce mouse embryonic and adult fibroblasts into pluripotent stem cells[29] were differentially expressed in our differentiated ADSCs, suggesting the successful differentiation of ADSCs into SC-like cells. According to the degree of SC differentiation, SCs were divided into SC precursor, myelinating SC and non-myelinating SC[30–32]. The SC markers of different differentiation degrees are different. The expression level of C-myc and OCT4 was exclusively observed in cultivated sciatic SC and not in freshly isolated sciatic nerves[33], suggesting that the pluripotency factors C-myc and OCT4 were increased in cultured SCs.

We subsequently performed RNAseq and transcriptome analyses to assess differentially expressed genes between primary cultured ADSCs and SC-like cells emerging upon ADSC differentiation. The global gene expression analysis showed that a large group of genes was differentially expressed between primary cultured and differentiated ADSCs. Our KEGG and GO analyses

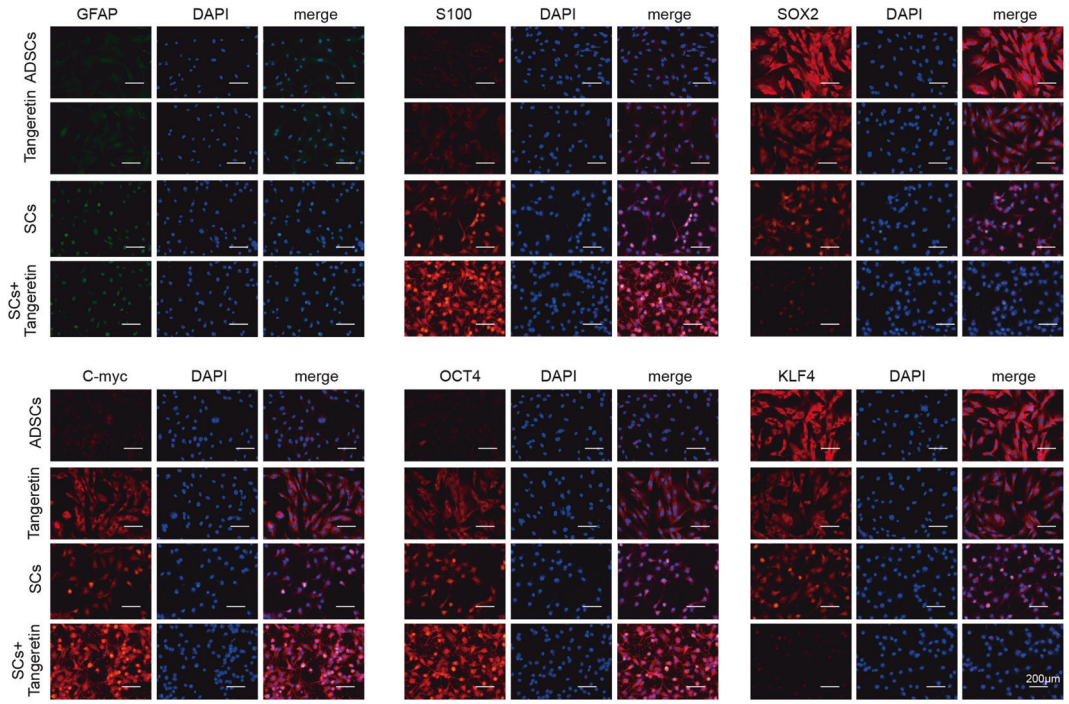

Fig. 5 The effect of Notch pathway on ADSC differentiation into SCs. The protein levels of GFAP, S100, SOX2, c-Myc, OCT4 and KLF4 in differentiated and primary cultured ADSCs treated with or without the Notch1 inhibitor tangeretin were detected using immunofluorescence.

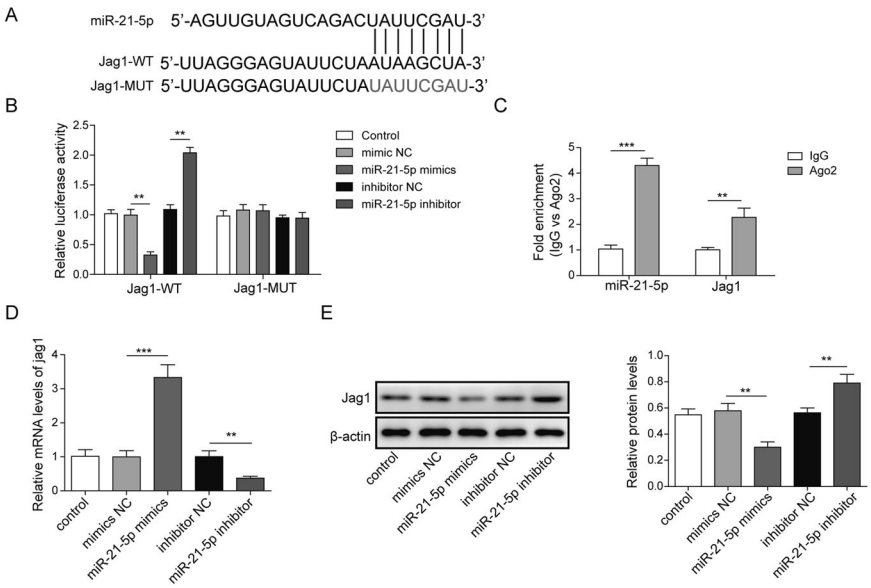

Fig. 6 miR-21-5p targets Rbpj. A The binding site for miR-21-5p in the Rbpj 3′UTR predicted by TargetScan. **B** Luciferase reporter activity of H293 cells transfected with control, miR-NC+3′UTR-WT, miR-21-5p+3′UTR-WT, miR-NC+3′UTR-Mut and miR-21-5p+3′UTR-Mu. **C** Interaction between miR-21-5p and Jag1 detected using RIP. **D** The expression levels of miR-21-5p were detected using qRT-PCR. **E** Jag1 protein levels detected using western blotting.

further revealed the involvement of the Notch signalling pathway in the differentiation of ADSCs into SCs.

Based on accumulating evidence, Notch signalling functions at different stages of SC development, acting both on neural crest stem cells[34] and mediating the generation of immature SCs from the precursor stage[35]. The addition of recombinant jagged1, an activator of Notch, to rat nerves after injury improves nerve regeneration and functional recovery[36]. Thus, the stimulation of Notch signalling in SCs might represent an interesting therapeutic strategy to efficiently promote nerve repair. Notch signalling pathways also contribute to the maintenance, regulation and differentiation of ADSCs obtained from mature adipose tissue. Specifically, inhibition of Notch signalling alters the ability of ADSCs to differentiate into various cell types, including adipogenic, osteogenic and neurogenic lineages[34,37–41]. On the other hand, activation of Notch signalling has been shown to inhibit the adipogenic differentiation of adipose-derived mesenchymal stem cell clones[42].

We analysed the binding site of miR-21-5p to further explain the molecular mechanism and validate the RNAseq results and found that it targeted the 3′-UTR of Jag1. Subsequently, experiments

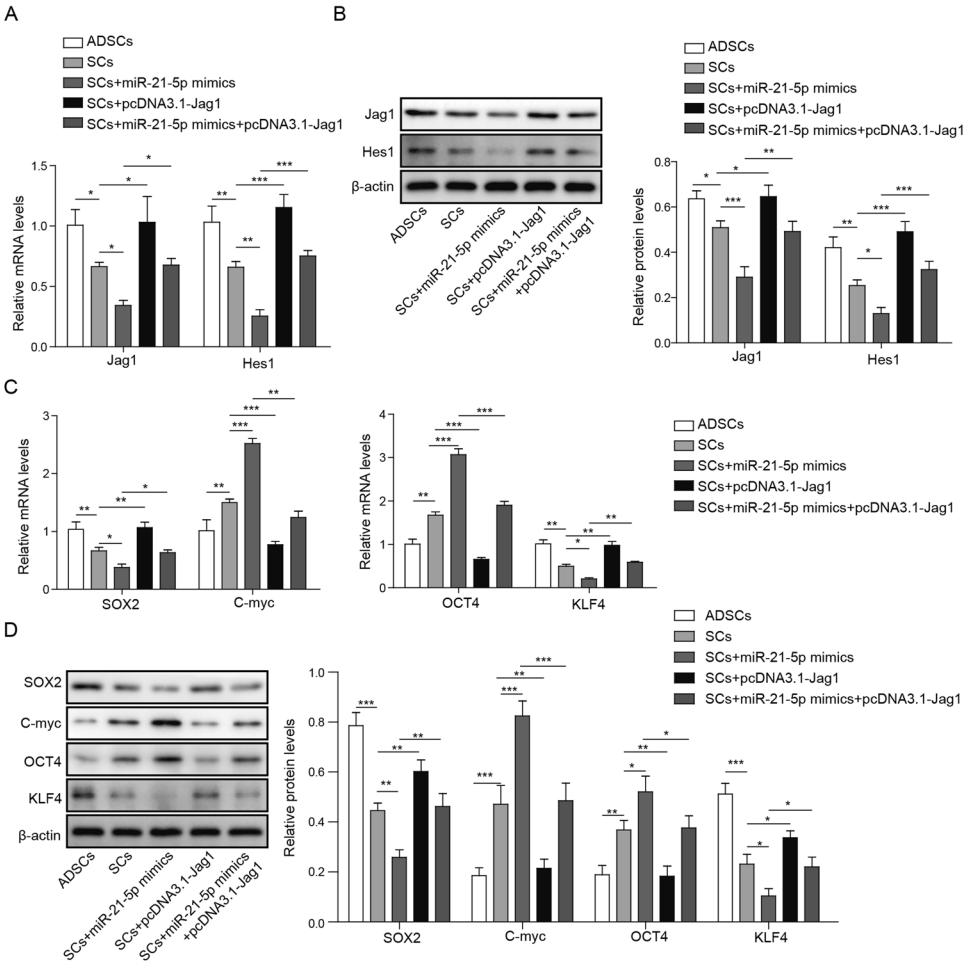

Fig. 7 miR-21-5p inhibits the Notch signalling pathway and regulates the differentiation of ADSCs into SCs by targeting Rbpj. A The expression levels of Jag1 and Hes1 after the transfection of lentiviral expression plasmids into ADSCs, SCs, SCs + miR-21-5p mimics, SCs + Jag1 overexpression plasmid (pcDNA3.1-Jag1) and SCs + miR-21-5p mimics + Jag1 overexpression plasmid were detected using qRT-PCR. **B** The corresponding levels of the Jag1 and Hes1 proteins in the indicated groups detected using western blotting. **C** The expression levels of SOX2, C-myc, OCT4 and KLF4 in the indicated groups were detected using qRT-PCR. **D** The corresponding levels of the SOX2, C-myc, OCT4 and KLF4 proteins in the indicated groups were detected using western blotting.

were designed, and the results confirmed the binding of miR-21-5p to Jag1 and subsequent regulation of its expression. Jag1 overexpression eliminated the regulatory function of miR-21-5p. These results prompted the hypothesis that miR-21-5p regulates Jag1 and then the Notch pathway. The differentiation of ADSCs into SC-like cells confirmed this hypothesis and provided a complete picture of the miR-21-5p regulatory pathway in the process.

In our study, important genes involved in the Notch signalling pathway, including Notch3–4, Jagged1–2 and Hes1, were differentially expressed in differentiated and primary cultures of ADSCs, as determined using RNA sequencing. qRT-PCR analyses further confirmed the upregulation of Notch1 and the downregulation of Jagged1 and Hes1 in differentiated ADSCs. In addition, inhibition of Notch activation with tangeretin, which prevents processing of the Notch receptor, upregulated C-myc and OCT4 expression and downregulated SOX2 and KLF4 expression in differentiated ADSCs. According to these data, the Notch signalling pathway plays an important role in maintaining ADSCs in a quiescent state, and the inhibition of this signalling pathway may induce ADSCs to differentiate into SCs.

Identification of Notch signalling as a critical pathway might lead to pragmatic clinical applications in peripheral regenerative therapeutics. In the future, in vivo experiment to elucidate the actual contribution the SCs differentiated from ADSCs to injured peripheral nerve tissue regeneration will be performed as one of our research directions. In addition, further studies are warranted to reveal the regulatory mechanism of noncoding RNAs during the differentiation process, as emerging evidence suggests the involvement of miRNAs in the regulation of the osteogenic and adipogenic differentiation of ADSCs[16,43]. Moreover, miRNAs have been shown to modulate the Notch signalling pathway in the cardiac differentiation of MSCs and in human gliogenesis[44]. These studies will provide novel insights into how Notch accurately regulates ADSC transdifferentiation into neural cells and will elucidate common mechanisms underlying Notch pathway regulation.

DATA AVAILABILITY

The data used to support the findings of this study are included within the article.

REFERENCES

1. Jain, S., Sharma, A. & Basu, B. In vitro cytocompatibility assessment of amorphous carbon structures using neuroblastoma and Schwann cells. *J. Biomed. Mater. Res. B Appl. Biomater.* **101**, 520–531 (2013).
2. Kashani, I. R. et al. Schwann-like cell differentiation from rat bone marrow stem cells. *Arch. Med. Sci.* **7**, 45–52 (2011).

3. Wakao, S. et al. Long-term observation of auto-cell transplantation in non-human primate reveals safety and efficiency of bone marrow stromal cell-derived Schwann cells in peripheral nerve regeneration. *Exp. Neurol.* **223**, 537–547 (2010).
4. Diaz Quiroz, J. F. & Echeverri, K. Spinal cord regeneration: where fish, frogs and salamanders lead the way, can we follow? *Biochem. J.* **451**, 353–364 (2013).
5. Zavan, B. et al. Neural potential of a stem cell population in the adipose and cutaneous tissues. *Neurol. Res.* **32**, 47–54 (2010).
6. Heidari, B. et al. Comparison of proliferative and multilineage differentiation potential of sheep mesenchymal stem cells derived from bone marrow, liver, and adipose tissue. *Avicenna. J. Med. Biotechnol.* **5**, 104–117 (2013).
7. Mehrkens, A. et al. Intraoperative engineering of osteogenic grafts combining freshly harvested, human adipose-derived cells and physiological doses of bone morphogenetic protein-2. *Eur. Cells Mater.* **24**, 308–319 (2012).
8. He, F. & Pei, M. Extracellular matrix enhances differentiation of adipose stem cells from infrapatellar fat pad toward chondrogenesis. *J. Tissue Eng. Regen. Med.* **7**, 73–84 (2013).
9. Butala, P. et al. Endogenous stem cell therapy enhances fat graft survival. *Plast. Reconstr. Surg.* **130**, 293–306 (2012).
10. Carvalho, P. H. et al. Differentiation of adipose tissue-derived mesenchymal stem cells into cardiomyocytes. *Arq. Bras. Cardiol.* **100**, 82–89 (2013).
11. Pavlova, G. et al. In vitro neuronal induction of adipose-derived stem cells and their fate after transplantation into injured mouse brain. *Curr. Med. Chem.* **19**, 5170–5177 (2012).
12. De Ugarte, D. A. et al. Comparison of multi-lineage cells from human adipose tissue and bone marrow. *Cells Tissues Organs* **174**, 101–109 (2003).
13. De Ugarte, D. A. et al. Differential expression of stem cell mobilization-associated molecules on multi-lineage cells from adipose tissue and bone marrow. *Immunol. Lett.* **89**, 267–270 (2003).
14. Strem, B. M. et al. Multipotential differentiation of adipose tissue-derived stem cells. *Keio. J. Med.* **54**, 132–141 (2005).
15. Razavi, S., Ahmadi, N., Kazemi, M., Mardani, M. & Esfandiari, E. Efficient transdifferentiation of human adipose-derived stem cells into Schwann-like cells: a promise for treatment of demyelinating diseases. *Adv. Biomed. Res.* **1**, 12 (2012).
16. Luo, L., Hu, D. H., Yin, J. Q. & Xu, R. X. Molecular mechanisms of transdifferentiation of adipose-derived stem cells into neural cells: current status and perspectives. *Stem Cells Int.* **2018**, 5630802 (2018).
17. Kingham, P. J. et al. Adipose-derived stem cells differentiate into a Schwann cell phenotype and promote neurite outgrowth in vitro. *Exp. Neurol.* **207**, 267–274 (2007).
18. Gao, S. et al. Different methods for inducing adipose-derived stem cells to differentiate into Schwann-like cells. *Arch. Med. Sci.* **11**, 886–892 (2015).
19. Razavi, S. et al. Effect of leukemia inhibitory factor on the myelinogenic ability of Schwann-like cells induced from human adipose-derived stem cells. *Cell. Mol. Neurobiol.* **33**, 283–289 (2013).
20. Chi, G. F., Kim, M. R., Kim, D. W., Jiang, M. H. & Son, Y. Schwann cells differentiated from spheroid-forming cells of rat subcutaneous fat tissue myelinate axons in the spinal cord injury. *Exp. Neurol.* **222**, 304–317 (2010).
21. Xu, Y. et al. Neurospheres from rat adipose-derived stem cells could be induced into functional Schwann cell-like cells in vitro. *BMC Neurosci.* **9**, 21 (2008).
22. Fu, X. et al. Induction of adipose-derived stem cells into Schwann-like cells and observation of Schwann-like cell proliferation. *Mol. Med. Rep.* **14**, 1187–1193 (2016).
23. Fuhrmann, D., Mernberger, M., Nist, A., Stiewe, T. & Elsasser, H. P. Miz1 controls schwann cell proliferation via H3K36(me2) demethylase Kdm8 to prevent peripheral nerve demyelination. *J. Neurosci.* **38**, 858–877 (2018).
24. Dobin, A. et al. STAR: ultrafast universal RNA-seq aligner. *Bioinformatics* **29**, 15–21 (2013).
25. Love, M. I., Huber, W. & Anders, S. Moderated estimation of fold change and dispersion for RNA-seq data with DESeq2. *Genome Biol.* **15**, 550 (2014).
26. Marappagounder, D., Somasundaram, I., Dorairaj, S. & Sankaran, R. J. Differentiation of mesenchymal stem cells derived from human bone marrow and subcutaneous adipose tissue into pancreatic islet-like clusters in vitro. *Cell. Mol. Biol. Lett.* **18**, 75–88 (2013).
27. Liu, G. B. et al. Adipose-derived stem cells promote peripheral nerve repair. *Arch. Med. Sci.* **7**, 592–596 (2011).
28. Bai, X. et al. Genetically selected stem cells from human adipose tissue express cardiac markers. *Biochem. Biophys. Res. Commun.* **353**, 665–671 (2007).
29. Takahashi, K. & Yamanaka, S. Induction of pluripotent stem cells from mouse embryonic and adult fibroblast cultures by defined factors. *Cell* **126**, 663–676 (2006).
30. Jessen, K. R. & Mirsky, R. The origin and development of glial cells in peripheral nerves. *Nat. Rev. Neurosci.* **6**, 671–682 (2005).
31. Liu, Z. et al. Specific marker expression and cell state of Schwann cells during culture in vitro. *PloS One* **10**, e0123278 (2015).
32. Jessen, K. R., Mirsky, R. & Lloyd, A. C. Schwann cells: development and role in nerve repair. *Cold Spring Harb. Perspect. Biol.* **7**, a020487 (2015).
33. Widera, D. et al. Schwann cells can be reprogrammed to multipotency by culture. *Stem Cells Dev.* **20**, 2053–2064 (2011).
34. Joseph, N. M. et al. Neural crest stem cells undergo multilineage differentiation in developing peripheral nerves to generate endoneurial fibroblasts in addition to Schwann cells. *Development* **131**, 5599–5612 (2004).
35. Woodhoo, A. et al. Notch controls embryonic Schwann cell differentiation, postnatal myelination and adult plasticity. *Nat. Neurosci.* **12**, 839–847 (2009).
36. Wang, J. et al. Effect of active Notch signaling system on the early repair of rat sciatic nerve injury. *Artif. Cells Nanomed. Biotechnol.* **43**, 383–389 (2015).
37. Cornell, R. A. & Eisen, J. S. Notch in the pathway: the roles of Notch signaling in neural crest development. *Semin. Cell Dev. Biol.* **16**, 663–672 (2005).
38. Taylor, M. K., Yeager, K. & Morrison, S. J. Physiological Notch signaling promotes gliogenesis in the developing peripheral and central nervous systems. *Development* **134**, 2435–2447 (2007).
39. Kingham, P. J., Mantovani, C. & Terenghi, G. Notch independent signalling mediates Schwann cell-like differentiation of adipose derived stem cells. *Neurosci. Lett.* **467**, 164–168 (2009).
40. Huang, Y. et al. gamma-secretase inhibitor induces adipogenesis of adipose-derived stem cells by regulation of Notch and PPAR-gamma. *Cell Prolif.* **43**, 147–156 (2010).
41. Jiang, R. et al. The long noncoding RNA lnc-EGFR stimulates T-regulatory cells differentiation thus promoting hepatocellular carcinoma immune evasion. *Nat. Commun.* **8**, 15129 (2017).
42. Osathanon, T., Subbalekha, K., Sastravaha, P. & Pavasant, P. Notch signalling inhibits the adipogenic differentiation of single-cell-derived mesenchymal stem cell clones isolated from human adipose tissue. *Cell. Biol. Int.* **36**, 1161–1170 (2012).
43. Chen, J. et al. The role of miRNAs in the differentiation of adipose-derived stem cells. *Curr. Stem Cell Res. Ther.* **9**, 268–279 (2014).
44. Patterson, M. et al. let-7 miRNAs can act through notch to regulate human gliogenesis. *Stem Cell Rep.* **3**, 758–773 (2014).

AUTHOR CONTRIBUTIONS

LY and WW: designed the study. LY, X-MS and ZW: conducted the experiments. ZW and KL: data analysis and statistical analysis. LY: paper preparation and editing. WW: paper review. All authors read and approved the final manuscript.

FUNDING

This work was supported by National Natural Science Foundation of China (No. 81601083).

COMPETING INTERESTS

The authors declare no competing interests.

ETHICS APPROVAL

All animal experiments and protocols were reviewed and approved by the Animal Care and Use Committee of the Third Xiangya Hospital of Central South University.

ADDITIONAL INFORMATION

Supplementary information The online version contains supplementary material available at https://doi.org/10.1038/s41374-021-00687-2.

Correspondence and requests for materials should be addressed to Wei Wang.

Reprints and permission information is available at http://www.nature.com/reprints

Publisher's note Springer Nature remains neutral with regard to jurisdictional claims in published maps and institutional affiliations.